ChemComm

Accepted Manuscript

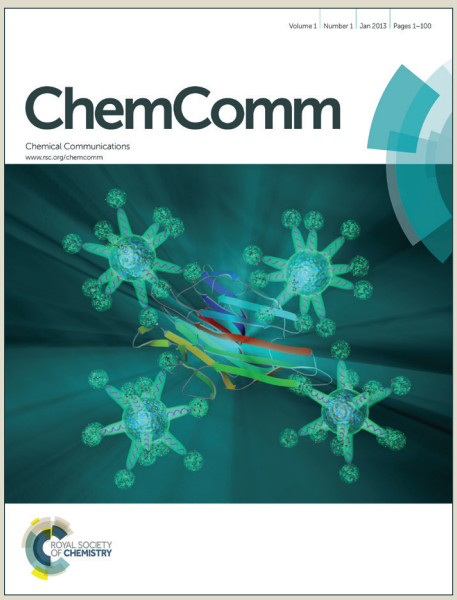

ROYAL SOCIETY OF CHEMISTRY

www.rsc.org/chemcomm

Journal Name

RSCPublishing

COMMUNICATION

www.rsc.org/

Cite this: DOI: 10.1039/x0xx00000x

Synergism between polyurethane and polydopamine in the synthesis of Ni-Fe alloy monoliths

Received 00th January 2012,
Accepted 00th January 2012

DOI: 10.1039/x0xx00000x

Thangavel Naresh Kumar[a], Santhana Sivabalan[b], Naveen Chandrasekaran*[b], Kanala Lakshminarasimha Phani*[a]

Herein, we report the first synthesis of light-weight macroporous 3-D alloy monolith of Ni-Fe/C using synergism between polydopamine (pDA) and polyurethane (pU); in situ formed polyurethane (pU) enables efficient mixing of pDA (carbon source) and Ni-FeO$_x$ resulting in Ni-Fe alloy monoliths at a temperature as low as ~600°C. The monolithic Ni-Fe/C exhibits enhanced oxygen evolution activity.

Metal aerogels are ultra-light weight three dimensional (3-D) architectures comprising of interconnected metallic nanoparticles with pore size less than 1000 nm. In the quest for alternatives to precious metals, metal aerogels appear to be ideally suited materials in the fields of biomedical, energy conversion and catalysis due to their enhanced properties.[1] Various synthetic strategies are in practice for the preparation of non-metallic aerogels such as silica[2], transition/rare earth metal oxides[3], polymer and their carbon derivatives.[4] However, only a few reports are available on the synthesis of metallic foams, namely foaming using blowing agents, chemical vapour deposition[5] or template-directed electrodeposition of metals[6], dealloying etc.[7] While a plethora of non-chemical routes are employed for the synthesis of metallic foams, only a few chemical approaches have been reported.[8] For example, Eychmüller group have reported on a different approach for the preparation of ordered macroporous mono-/bi-(noble)metallic aerogels, based on controlled aggregation of nanoparticles[9]. Enhanced electrocatalytic activity of these metal aerogels has also been demonstrated by this group[10]. Tappan et al. developed a procedure to synthesize porous metal foams by combustion synthesis.[11] Recently, metal aerogels were developed by Leventis et al[12] *via* sol-gel process by forming interpenetrating networks of metal oxide and polymer followed by pyrolysis under inert atmosphere to yield metallic aerogel. In these reports, organic polymers such as resorcinol-formaldehyde[4], polybenzoxazine[13] act as the carbon source in reducing metal oxide to porous metal aerogels. In this context, dopamine presents us with a polymerizable functional unit that is known to form stable and robust anchors on the surface of metal iron oxides[14]. While dopamine attracted attention as capping agent due to the stability and strength of the resultant five-membered metallocycle chelate and the ease with which it can be functionalized through amide bonds with other molecules[14], its polymer (pDA) formed by self-polymerization of dopamine under mild alkaline conditions (pH~8.0) appears especially relevant to metal aerogel synthesis with its excellent adhesion on diverse substrates (resulting in a few nanometers thick polymer films[15]). The –NH$_2$ and –OH functional groups on the pDA chain act as ligands to bond with metal oxides to form a core-shell type of structure of pDA-metal oxide or *vice-versa*.[16] In addition to the formation of core-shell structures with diverse materials such as metal oxides, metals and polymers, pDA can leave behind sp^2 carbon skeleton when pyrolyzed at higher temperatures under inert conditions.[17] The sp^2 carbon backbone similar to graphene, can readily reduce metal oxides to metals.[13] In electrocatalysis applications, nanoporosity may pose problems due to limited diffusion through the nanochannels as they hamper chemical manipulation of the metal foams. Even materials of moderate surface area were shown by Eychmüller group to be highly electrocatalytic in nature. A key challenge is to achieve a balance between active surface area and a continuous hierarchical macroporosity. It is thus imperative that (i) the metal aerogels/monoliths are supported on a conducting matrix preferably; and (ii) the chemical network should act both as a template and carbon source. We demonstrate in this work for the first time two polymeric matrices acting *in concert* to provide such an ideal network to achieve these objectives. More importantly, we report here the synthesis of *pure alloy particles supported on a carbon skeleton in monolithic form*.

In the present approach, we have demonstrated a synthetic route by coating pDA on Ni-FeO$_x$ aerogel followed by a top-coat with tri-isocyanate yielding a Ni-FeO$_x$@pDA-pU monolithic gel. In this hierarchical structure, pDA acts as the carbon source in reducing metal oxide to metal, whilst, pU formed by the reaction of –N=C=O with functional groups (–NH$_2$,–OH etc.,) present in pDA enables efficient mixing of pDA and Ni-FeO$_x$ resulting in Ni-Fe alloy monoliths at a temperature as low as ~600° C. The Ni-FeO$_x$ aerogels coated by individual pDA and tri-isocyanate lead to a mixture of metallic Ni and Fe_3O_4 particles. The obtained Ni-Fe alloy monoliths were found to be electrocatalytic towards the oxygen evolution reaction.

The nature of chemical functionalization of pDA-pU on Ni-FeO_x was confirmed by FTIR spectra of aerogels of Ni-FeO_x, Ni-FeO_x @pDA and Ni-FeO_x@pDA-pU (Fig.1). The neat Ni-FeO_x aerogels show their characteristic peaks at 3404, 1589, 1110 and 495 cm^{-1} assigned to broad ν OH, δ H_2O, δ OH and ν Ni-O or Fe-O respectively. In addition to Ni-O or Fe-O peak at 465 cm^{-1} already present in the Ni-FeO_x aerogel, FTIR spectra of Ni-FeO_x@pDA confirm the coordination of dopamine with Ni-FeO_x by the formation of new sharp peaks at 3395, 1621 and 1479 cm^{-1} corresponding to ν N-H, aromatic δ N-H and ν C=C, respectively. Successful functionalization of tri-isocyanate with $–NH_2$ and –OH functional groups present in pDA was confirmed by the appearance of new peaks at 2931, 1667 cm^{-1} attributed to aliphatic ν C-H and ν C=O from the pU linkage respectively. Similar chemical functionalization of pDA and pDA-pU was observed in NiO_x and FeO_x aerogels (Figs.S1 and S2 ESI†)

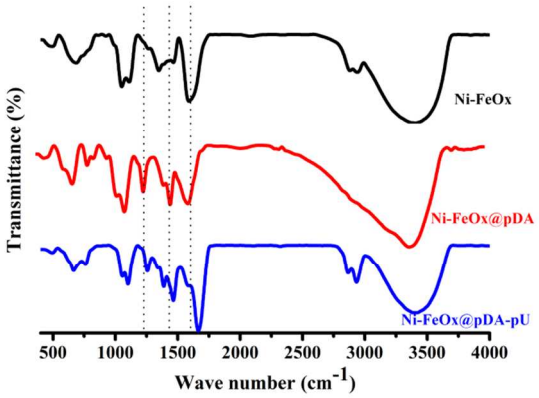

Figure 1: FTIR spectrum of Ni-FeO_x, Ni-FeO_x@pDA and Ni-FeO_x@pDA-pU

The Ni-FeO_x@pDA-pU aerogels were converted to Ni-Fe alloy monoliths by pyrolysis under flowing Ar at 800°C. The porosity values calculated using bulk and skeletal densities (0.81 and 3.64 g/cm^3) for Ni-Fe monoliths worked out to be 77%. The synergestic effect[18] of pDA and pU in the synthesis of Ni-Fe monoliths becomes evident in the results of x-ray diffractometry (Fig.2): Ni-FeO_x@pDA (or pU) shows diffraction patterns corresponding to metallic Ni at 44.94° (111), 51.96° (200) and crystalline Fe_3O_4 peaks at 35.66°(311), 43.21° (400) and 63.2° (440). On the other hand, Ni-FeO_x@pDA-pU pyrolyzed at different temperatures (400, 600°C) shows reflections corresponding to Ni-Fe alloy phase at 44.42° (111) in addition to Fe_3O_4 phase whereas, similar samples pyrolyzed at 800° C show complete formation of Ni-Fe alloy phase with the emergence of new peaks at 43.9° (111), 51.14° (200) and 75.31° (220) with no traces of oxides. Also, the XRD pattern matches with the standard patterns of $FeNi_3$ (ICDD # 00-038-0419). The crystallite size of Ni-Fe alloy determined using Scherrer's formula was found to be ~15 nm. Synergism between pDA and pU is further confirmed from the XRD pattern of NiO_x and FeO_x coated with individual polymers pDA and pU pyrolyzed at 800° C giving metallic Ni and Fe_3O_4 respectively (Fig.S3, ESI†). This unusual behavior of NiO_x and FeO_x coated with individual polymers pDA and pU may be explained as follows:

(a) Higher temperature required to reduce Fe (> 900° C)
(b) Formation of stable iron oxides (Fe_3O_4, FeO, γ-Fe_2O_3) as intermediates during the reduction of Fe_2O_3 to Fe.
X-ray diffraction patterns of Ni-FeO_x@pDA-pU pyrolyzed at 400º, 600º, and 800ºC indicates the formation of individual metallic (Ni, Fe) phases and Ni-Fe alloy phase as low as 400ºC, 600ºC respectively as shown in Fig 2. Alloy formation between Ni and Fe, known to occur at temperatures ~700°C invariably leads to mixed phases of alloy and metal oxides,[19] whereas in the present work complete alloy formation is observed at ~800°C with no traces of metal oxides (Fig.3). The early formation of Ni-Fe alloy phase at 600ºC and macroporosity can be deemed to:

1. Melting of aliphatic pU at a temperature <128ºC leads to the collapse of Ni-FeO_x@pDA network assisting in efficient mixing of pDA and Ni-FeO_x particles, in turn reducing the temperature required for Ni-Fe alloy phase formation.[12]
2. In addition to gases that evolve during pyrolysis of pDA, thermal decomposition of pU produces gases such as CO, NH_3. These can effectively reduce metal oxide to metal aiding the formation of macroporous carbon skeleton.[20] The presence of carbon enclosure on Ni-Fe monoliths is confirmed by the appearance of the characteristic D (1354 cm^{-1}) and G (1595 cm^{-1}) bands in Raman spectroscopy [Fig.S4 ESI†].

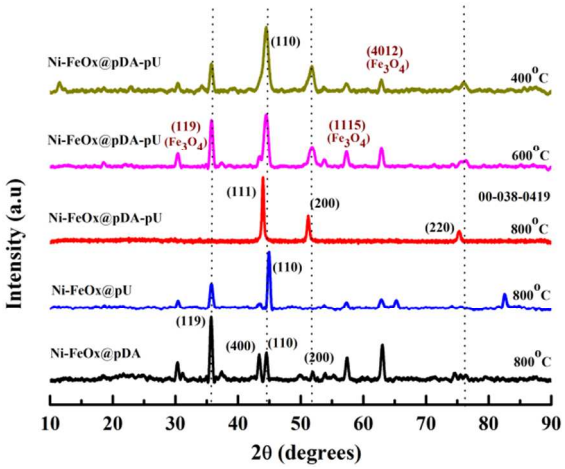

Figure 2: XRD patterns of Ni-FeO_x@pDA, Ni-FeO_x@pU and Ni-FeO_x@pDA-pU at different temperatures (400, 600 and 800°C)

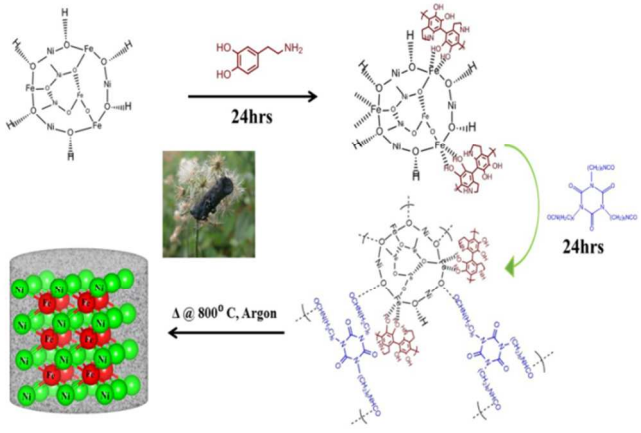

Figure 3: Schematic representation of Ni-Fe monolith synthesis (Photograph of Ni-Fe/C monolithic piece resting on dandelion flower parachute ball is given to show its light-weight)

It can be seen from the FESEM (Fig.4a) that Ni-Fe monoliths comprise particles of 100 nm size along with larger ones in the range of 1µm embedded on macroporous carbon (derived from pDA and pU).[12, 21] Consistent with the FE-SEM images, the N_2 sorption isotherm (Fig.4b) for Ni-Fe monoliths follows a typical type II isotherm for macroporous materials with a BET surface area of 6 m^2g^{-1}. Microscopically, Ni and Fe monoliths were found to have particles on the carbon backbone (Fig.S5 ESI†). Similar to the Ni-Fe monoliths, N_2 sorption isotherms for Ni and Fe show type II behavior characteristic of a macroporous structure (Fig. S6 ESI†)

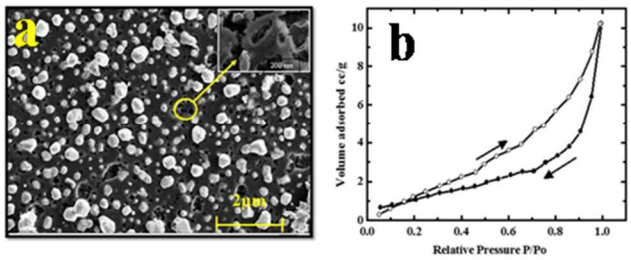

Figure 4: (a) FE-SEM image of Ni-Fe, magnification: 2µm (inset shows the zoomed part of the porous network); (b) BET isotherm of Ni-Fe monolith.

Incidentally, these macroporous Ni-Fe alloy monoliths are rendered electrically conducting due to the carbon skeleton derived from pDA-pU pyrolysis, befitting the requirement as carbon-supported electrocatalysts. In the present work, we take advantage of this property to examine electrocatalysis of oxygen evolution reaction (OER) considering the recent interest in the development of non-noble metal electrocatalysts.[22, 23]

Fig.5a displays the cyclic voltammograms of Ni, Fe and Ni-Fe@GC electrode in 0.1 M KOH. The redox peak pair at E_{pa} = 0.44 mV; E_{pc} = 0.35 mV vs Hg/HgO in the voltammetric response of Ni@GC can be ascribed to the $Ni(OH)_2$/NiOOH transformation.[24] In agreement with the previous reports,[25] Fe@GC showed no redox characteristics since the transformation of Fe(II)/Fe(III) occurs at higher overpotentials. Consistent with the reports in ref.[26], Ni-Fe@GC displays an anodic shift (~60 mV) of ($Ni(OH)_2$/NiOOH) redox caused by the presence of Fe. Fig.5b shows the representative linear sweep voltammograms of all three electrodes in 0.1 M KOH illustrating its electrocatalytic activity towards oxygen evolution

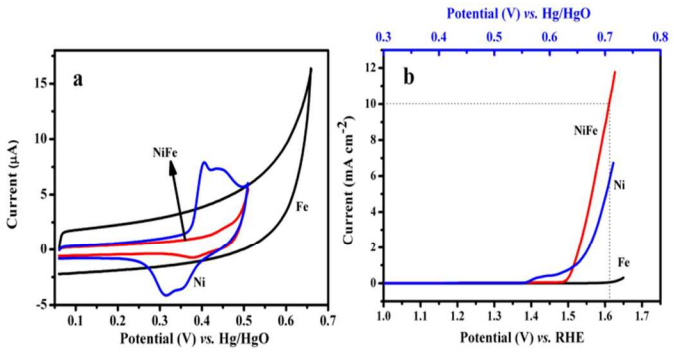

Figure 5: (a) Cyclic; (b) Linear sweep voltammetric responses of Fe, Ni and Ni-Fe monolith (supported on glassy carbon surface) in 0.1M KOH at 1600 rpm. Scan rate: 5 mV/sec

reaction. A steep increase in current is observed for both Ni and Ni-Fe@GC at 0.60V, whereas, Fe@GC displayed OER at potentials beyond 0.70V. At an overpotential of 375 mV vs RHE, Ni-Fe@GC modified electrode yields a current density of 10 mA/cm^2. This value is comparable or even superior to the transition metal based OER catalysts reported elsewhere [Table S1: (i) Ni/Au, 10 mA/cm^2@350 mV[27], (ii) Ni-FeO_x@Au, 10 mA/cm^2@280 mV[28]]. Mechanistic information on OER was obtained by analysing Tafel relationship, η = a ± b logi. The *iR* corrected Tafel plots shown in [Fig S7 ESI†] reveals values of 51 mV/dec and 55 mV/dec for Ni and Fe films, whereas, Ni-Fe film displayed a tafel slope of 42 mVdecade^{-1}. This lowered Tafel slope suggests that the Ni-Fe/C-monolithic electrocatalyst is on par with the benchmark IrO_2 catalyst.[29] The presence of Fe providing more active sites for OH adsorption on Ni-Fe electrodes in turn changing the rate determining step from the discharge of hydroxyl ions to recombination of oxygen radicals as evident from the decrease in the tafel slope value.[30] The enhanced access of electrolyte to the active site is facilitated by the three dimensional assemblies of Ni-Fe particles embedded on macroporous carbon (diffusion is no longer limiting in this case).[31]

Additionally, turn-over frequency (TOF) was calculated for Ni and Ni-Fe films using the relationship,

$$TOF_{max} = I^* N_A / 4N_{atoms}F$$

where, I, N_A, $N_{atoms,}$ F represents the current obtained at 700 mV, Avagadro number, number of atoms at the surface and Faraday constant respectively. A turn-over frequency of 125 s^{-1} (and a Faradaic efficiency of 97% deduced from the analysis of data collected in the rotating ring disk electrode voltammetry, (Table S2 & Fig.S8 ESI†) obtained for the Ni-Fe film, ca. is 5 times higher relative to that of a Ni film (25 s^{-1}).[27] Enhanced current density at a constant overpotential, decrease in tafel slope and high TOF values for Ni-Fe films clearly indicate increased catalytic activity towards OER.

In summary, we have developed a facile synthetic strategy and demonstrated the synergistic effect of pDA and pU in the preparation of three dimensional (3-D) Ni-Fe alloy embedded on a macroporous carbon. XRD analysis of the NiO_x, FeO_x Ni-FeO_x@pDA-pU pyrolyzed at 800^o C indicates complete formation of metallic Ni, Fe and Ni-Fe alloy respectively. Here, pDA acts as the carbon source and pU aids efficient mixing of particles of Ni-FeO_x and pDA, in turn bringing down the activation energy required for alloy formation. The as obtained Ni-Fe alloy monoliths were found to be free-standing with a porosity of 77%. We found that similar synergism is operative in the synthesis of Fe-Co/C monoliths (Fig.S9 ESI†), demonstrating its general applicability. The Ni-Fe alloy monolith shows excellent activity towards OER in 0.1 M KOH with a current density of 10 mA/cm^2 at overpotential of 375 mV *vs* RHE and a Tafel slope of 42 mV dec^{-1} relative to their metallic counterparts.

It may be possible to list three types of advantages arising from these metallic monoliths: (i) macroporosity of these monoliths offers the advantage of complete utilization of the catalytic surface; and (ii) monolithic nature helps overcoming the disadvantages of immobilizing the transition metal catalytic particles on a (carbon) support. As pDA is very adherent, by its nature, it will be a facile way of forming thin films of metal monoliths on pDA-coated substrates prior to carbonization.[17b] We are currently pursuing these approaches to establish intimate contact of the catalyst layer to the substrate material from a practical point of view. The high carbon content ensures that the reaction at high rates is not limited by either the electronic conductivity or ionic diffusion within the electrode composite.

Notes and references

[a] Mr.Thangavel Naresh Kumar, Dr. Kanala Lakshminarasimha Phani
Nanoscale Electrocatalysis Group, Electrodics & Electrocatalysis Division, CSIR-Central Electrochemical Research Institute
Karaikudi-630006 India
Fax: (+) 914565227779, 227713
E-mail: kanalaphani@yahoo.com; klnphani@cecri.res.in
[b] Mr. Santhana Sivabalan, Dr.Naveen Chandrasekaran
Electroplating & Metal Finishing Technology Division
CSIR-Central Electrochemical Research Institute, Karaikudi-06
E-mail: naveen@cecri.res.in; naveenumr@gmail.com

Acknowledgements: TNK thanks India's CSIR for a senior research fellowship. KLNP thanks Mr. P. Esakki Karthik for useful discussions and acknowledges support from India's DST for a grant under Australia-India Strategic Research Fund [DST/INT/AUS/P-43/2011] and CSIR programme under MULTIFUN: CSC-0101.
[Electronic supplementary information are available: Chemicals, experimental procedure, electrochemical characterization, Tafel plots, TOF calculation, RRDE measurements, and characterization such as FTIR, FE-SEM, XRD, BET surface area and Laser Raman data. See DOI: 10.1039/c000000x]

1. B. C. Tappan, S. A. Steiner, and E. P. Luther, *Angew. Chem. Int. Ed. Engl.*, 2010, **49**, 4544.
2. (a) N. Hüsing and U. Schubert, *Angew. Chemie Int. Ed.*, 1998, **37**, 22; (b) L. L. Hench and J. K. West, *Chem. Rev.*, 1990, **90**, 33.
3. (a) N. Leventis, P. Vassilaras, E. F. Fabrizio, and A. Dass, *J. Mater. Chem.*, 2007, **17**, 1502; (b) A. E. Gash, T. M. Tillotson, J. H. Satcher,, J. F. Poco, L. W. Hrubesh, and R. L. Simpson, *Chem. Mater.*, 2001, **13**, 999; (c) A. E. Gash, J. H. Satcher, and R. L. Simpson, *J. Non. Cryst. Solids.*, 2004, **350**, 145.
4. (a) S. Mulik, C. S. Leventis, and N. Leventis, *Chem. Mater.*, 2007, **19**, 6138; (b) R. W. Pekala, C. T. Alviso, F. M. Kong, and S. S. Hulsey, *J. Non. Cryst. Solids.*, 1992, **145**, 90; (c) R. Pekala, *J. Mater. Sci.*, 1989, **24**, 3221; (d) N. Leventis, C. S. Leventis, N. Chandrasekaran, S. Mulik, Z. J. Larimore, H. Lu, G. Churu, and J. T. Mang, *Chem. Mater.*, 2010, **22**, 6692; (e) A. Rigacci, J. C. Marechal, M. Repoux, M. Moreno, and P. Achard, *J. Non. Cryst. Solids.*, 2004, **350**, 372; (f) G. C. Ruben and R. W. Pekala, *J. Non. Cryst. Solids.*, 1995, **186**, 219.
5. (a) V. Paserin, S. Marcuson, J. Shu, and D. S. Wilkinson, *Adv. Eng. Mater.*, 2004, **6**, 454; (b) O. Olurin, *Compos. Sci. Technol.*, 2003, **63**, 2317.
6. (a) K. Zhang, X. Tan, W. Wu, and Y. Tang, *Mater. Res. Bull.*, 2013, **48**, 3499; (b) S. Cherevko, X. Xing, and C.H. Chung, *Electrochem. Commun.*, 2010, **12**, 467; (c) N. D. Nikolić, G. Branković, M. G. Pavlović, and K. I. Popov, *J. Electroanal. Chem.*, 2008, **621**, 13; (d) G. W. Nyce, J. R. Hayes, A. V Hamza, and J. H. Satcher, *Chem. Mater.*, 2007, **19**, 344.
7. (a) R. Morrish and A. J. Muscat, *Chem. Mater.*, 2009, **21**, 3865; (b) Z. Qi, C. Zhao, X. Wang, J. Lin, W. Shao, Z. Zhang, and X. Bian, *J. Phys. Chem. C*, 2009, **113**, 6694; (c) Z. Zhang, Y. Wang, Z. Qi, W. Zhang, J. Qin, and J. Frenzel, *J. Phys. Chem. C.*, 2009, **113**, 12629.
8. (a) Z. Hua, Y. Deng, K. Li, and S. Yang, *Nanoscale Res. Lett.*, 2012, **7**, 129; (b) N. Kränzlin and M. Niederberger, *Adv. Mater.*, 2013, **25**, 5599.
9. (a) L. Lu, A. Eychmüller, *Acc.Chem.Res*., 2008, **41**, 244 (b) N. Gaponik, A.K. Herrmann, A. Eychmüller, *J. Phys. Chem. Lett*., 2012, **3,** 8
10. (a)D.Wen,A.K.Hermann,L.Borchardt,F.Simon,W.Liu,S.Kaskel,A. Eychmuller, *J.Am.Chem.Soc.,* 2014, **136,** 2727 (b) W.Liu, A.K.Hermann, D.Geiger, L.Borchdart, F.Simon, A.Eychmuller, *Angew.Chem.Int.Ed.,* 2012, **51**, 5743
11. B. C. Tappan, M. H. Huynh, M. a Hiskey, D. E. Chavez, E. P. Luther, J. T. Mang, and S. F. Son, *J. Am. Chem. Soc.*, 2006, **128**, 6589.
12. (a) N. Leventis, N. Chandrasekaran, A. G. Sadekar, S. Mulik, and C. Sotiriou-Leventis, *J. Mater. Chem.*, 2010, **20**, 7456; (b) N. Leventis, N. Chandrasekaran, C. S. Leventis, and A. Mumtaz, *J. Mater. Chem.*, 2009, **19**, 63; (c) N. Leventis, N. Chandrasekaran, A. G. Sadekar, C. S. Leventis, and H. Lu, *J. Am. Chem. Soc.*, 2009, **131**, 4576.
13. (a) S. Mahadik-Khanolkar, S. Donthula, A. Bang, C. Wisner, C. Sotiriou-Leventis, and N. Leventis, *Chem. Mater.*, 2014, **26**, 1318; (b) S. Mahadik-Khanolkar, S. Donthula, C. Sotiriou-Leventis, and N. Leventis, *Chem. Mater.*, 2014, **26**, 1303.
14. (a) C.J. Xu, K.M. Xu, H.W.Gu, R.K. Zheng, H. Liu, X.X.Zhang, Z.H.Guo, B. Xu, *J. Am. Chem. Soc*., 2004, **126**, 9938; (b) M.D. Shultz, J.U. Reveles, S.N. Khanna, E.E. Carptenter, *J. Am. Chem. Soc*., 2007, **129**, 2482
15. H. Lee, S. M. Dellatore, W. M. Miller, and P. B. Messersmith, *Science(AAAS)*, 2007, **318**, 426.
16. (a) M. Martín, P. Salazar, R. Villalonga, S. Campuzano, J. M. Pingarrón, and J. L. González-Mora, *J. Mater. Chem. B.*, 2014, **2**, 739; (b) H.P. Peng, R.P. Liang, L. Zhang, and J.D. Qiu, *Biosens. Bioelectron.*, 2013, **42**, 293; (c) T. Zeng, X. Zhang, H. Niu, Y. Ma, W. Li, and Y. Cai, *Appl. Catal. B Environ.*, 2013, **134-135**, 26; (d) J.J. Feng, P.P. Zhang, A.J. Wang, Q.C. Liao, J.L. Xi, and J.R. Chen, *New J. Chem.*, 2012, **36**, 148.
17. (a) K. Ai, Y. Liu, C. Ruan, L. Lu, and G. M. Lu, *Adv. Mater.*, 2013, **25**, 998; (b) R. Li, K. Parvez, F. Hinkel, X. Feng, and K. Müllen, *Angew. Chemie Int.Ed.*, 2013, **125**, 5645.
18. In a restricted sense, the contributions of pDA and pU can be considered as synergistic effect since only in presence of both, carbonization, metal oxide reduction and alloy formation take place. However, in order to fully justify the effect, detailed calorimetric measurements are required, considering the energetics involved in the reduction of metal oxides to metals and alloy formation.
19. G. Li, Y. Guo, X. Sun, T. Wang, J. Zhou, and J. He, *J. Phys. Chem. Solids.*, 2012, **73**, 1268.
20. (a) G. Watt and W. Fernelius, *J. Am. Chem. Soc.*, 1939, **61**, 2502; (b) M. Paabo and B. Levin, *Fire Mater.*, 1987, **11**, 1.
21. S. Mulik, C. Sotiriou-Leventis, and N. Leventis, *Chem. Mater.*, 2008, **20**, 6985.
22. Y. J. Sa, K. Kwon, J. Y. Cheon, F. Kleitz, and S. H. Joo, *J. Mater. Chem. A.*, 2013, **1**, 9992.
23. The affinity of iron to water helps the formation of Ni=O at lower overpotentials. The so-called "oxo-wall" prohibits the formation of a formal Ni=O double bond (*D.J. Wasylenko, C. Ganesamoorthy, J.B.-Garcia, C.P. Berlinguette, Chem. Comm., 2011, 47, 4249*), whereas Fe-oxo bond (by the reaction of water) is known to form readily and thus this cooperative effect will result in the decomposition of the metal-oxo complex to yield molecular oxygen.
24. R. Kostecki, *J. Electrochem. Soc.*, 1997, **144**, 485.
25. R. L. Doyle and M. E. G. Lyons, *J. Electrochem. Soc.*, 2013, **160**, H142.
26. (a) L. Trotochaud, S. L. Young, J. K. Ranney, and S. W. Boettcher, *J. Am. Chem. Soc.*, 2014, **136**, 6744; (b) J. Landon, E. Demeter, and N. İnoğlu, *ACS Catalysis.,* 2012, **2**, 1793.
27. C. C. L. McCrory, S. Jung, J. C. Peters, and T. F. Jaramillo, *J. Am. Chem. Soc.*, 2013, **135**, 16977.
28. M. Lyons, *Int. J. Electrochem. Sci.*, 2008, **3**, 1463.
29. M. W. Louie and A. T. Bell, *J. Am. Chem. Soc.*, 2013, **135**, 12329.
30. D. A. Corrigan, *J. Electrochem. Soc.*, 1987, **134**, 377.
31. It is observed that most metallic aerogels reported so far by Eychmüller group are of moderate surface area, typically in the range of 50-150 m^2/g and in the case of Ag-foams (*Chem. Mater., 2014, 26, 4064-4067*), the value is around 20 m^2/g. According to Eychmüller, low surface area materials also enhance the electrocatalytic activity as materials of macroporous network provide easy access to OH^- ions towards active sites present inside the network. This effect was exemplified in the case of Pd aerogels for bio-electrocatalytic glucose oxidation *(J. Am. Chem. Soc. 2014, 136, 2727−2730).*

Table of content